scientific reports

Check for updates

OPEN

HOXD1 regulates neural crest cells differentiation and polycerate development in sheep

Cheng Zhang[1,2], Shuhong Zhang[1], Huifeng Xu[2], Guan Wang[1], Huan Zhang[1,2], Tenggang Di[1,2], Liming Tian[1,3], Menghan Chang[1,2], Fengyi Gao[1], Ming Li[2]✉ & Guangli Yang[1]✉

The polycerate trait in sheep is a complex phenotype regulated by polygenes. However, the mechanism behind multi-horned traits development and growth remains unclear. In this study, neural crest cells (NCCs) were isolated from mouse embryos, and the *HOXD1* (*Homeobox D1*) gene was overexpressed in these cells to identify its function. Transcriptome analysis was performed to explore the key signaling pathway involved in forming the multi-horned traits in sheep. The results showed that the *HOXD1* induced epithelial-to-mesenchymal transition (EMT) in mouse neural crest primary cells, affecting their migration but without significantly influencing proliferation. Furthermore, signaling pathway analysis suggested that *HOXD1* may inhibit NCC proliferation by modulating *Wnt* rather than *TGF-β* signaling. Transcriptome analysis revealed that the *HOXD1* gene affected the extracellular matrix of CXC family regulatory cells and promoted NCC differentiation. These findings provide a theoretical basis for further investigation into the regulation of multi-horned traits growth and development in sheep.

Keywords Sheep, Polycerate trait, Neural crest cells, *HOXD1* gene, Chemokine CXC

The sheep have diverse horn phenotypes, such as polled, two-horned, and polycerate. Polyceraty is an ancient genetic characteristic in sheep. In modern large-scale animal husbandry, multi-horned traits can complicate production management. A common issue is that individual sheep fight, leading to injuries and excessive energy use, affecting the growth and development of the animal. Multi-horned sheep play a role in maintaining biology diversity and serve as valuable resources for ornamental purposes and scientific research. Just as the adaptability of domestic animals to the environment under different climatic conditions[1].

Genome-wide association studies have mapped candidate genes to several chromosome regions in polycerate sheep populations[2–6]. Thus, polyceraty is a complex trait regulated by multiple genes. Allais-Bonne et al. (2021) examined various polycerate gene mutants and found that they cause the division of horn bud primordia at specific genetic loci[7]. The *HOXD1* gene plays a key role in structuring headgear and determining the number and location of horns in Bovidae[7]. The *Hox* gene cluster is highly conserved across animals and influence symmetrical embryos development. The *Hox* transcription factor acts as a pioneer factor[8], initiating the transcription of certain genes and regulating cell proliferation, metastasis, invasion, and angiogenesis[9,10]. *HOXD1*, *HOXD8*, and *HOXD10* have cancer-inhibiting function, preventing cancer cells spread and promoting apoptosis[11–13]. In multi-horned traits, a 4 bp deletion in *HOXD1* is entirely linked to controlling fetal development in sheep[7]. This deletion determines the polycerate traits in the Chinese Sishui fur sheep breed (Fig. S1), where the multi-horned phenotype follows a dominant inheritance pattern[14]. However, the mechanisms behind the development and growth of of the multi-horned traits in sheep remain unclear.

Some studies have shown that all candidate genes for horn traits relate to cell migration and differentiation. In vitro experiments indicate that *RXFP2* expression in periosteum cells of the horn stalk increases with rising androgen levels, affecting cell proliferation and differentiation[15]. *TWIST1* was shown to influence horn development in cattle, offering an opportunity to better understand horn ontogenesis[16]. The loss of *TWIST1* regulatory function causes abnormal differentiation of neural crest cells (NCCs)[17]. In human cancer research, *TWIST1* induces epithelial-to-mesenchymal transition (EMT), driving cancer metastasis, while its N-terminus antagonizes *TWIST1*-regulated gene expression, cancer growth, and metastasis[18]. For *HOXD1*, a candidate gene for the polycerate trait, loss-of-function and gain-of-function experiments showed that it inhibited cell proliferation, cell cycle, and the TGF-β signaling pathway[11].

[1]College of Biology and Food, Shangqiu Normal University, Shangqiu 476000, China. [2]College of Animal Science and Technology, Henan Agricultural University, Zhengzhou 450002, China. [3]College of Animal Science and Technology, Gansu Agricultural University, Lanzhou 730070, China. ✉email: liming@henau.edu.cn; guangliyang@163.com

These findings suggest that candidate gene cause hornless trait or misshapen horns by the disrupting normal differentiation or hindering horn bud migration. The multi-horned traits likely relate to cell migration and differentiation during early horn base development. To explore the mechanisms behind the multi-horned traits in sheep, craniofacial NCCs from C57BL/6 mouse embryos were isolated and cultured. Overexpression technology was then used to increase *HOXD1* expression in mouse NCCs to verify its function. Transcriptome sequencing was employed to identify key signaling pathways involved in the effect of *HOXD1* overexpression on polyceraty development in sheep. These results are significant for molecular marker breeding in polycerate sheep and for understanding the development of multi-horned traits.

Materials and methods

Animals

Pregnant C57BL/6 mice were purchased from the Henan Sikbers Biotechnology Co., Ltd (Nanyang, China). Experimental animal selection and research were conducted in accordance with the ARRIVE guidelines. The animal care and use guidelines put forth by the Ministry of Science and Technology of China (Guidelines on Ethical Treatment of Experimental Animals (2006) No. 398) were followed for this study, and all experiments were approved by the Ethics Committee of the Shangqiu Normal University (Shang (2022) No. 24). All methods were performed in accordance with the relevant guidelines and regulations.

Isolation of NCCs

Craniofacial NCCs were isolated and cultured at embryonic day 11.5 (E11.5). Pregnant mice were euthanized by cervical dislocation, and the uterus was collected and placed in a pre-cooled PBS dish containing 2% monoclonal antibody. The myometrium, decidua, and other tissues were carefully removed from the embryo. The embryo body was removed at the neck, and the first branchial arch was excised and chopped into small tissue pieces (about 1 mm^3) under a stereo microscope (Olympus, Tokyo, Japan). The tissues were transferred to a sterile environment, washed with PBS, placed in a cell culture dish, with complete culture medium, and incubated at 37 °C and 5% CO_2 for 30 min. After 48 h, the tissue block was removed, and the medium was replaced. The tissue could be repeatedly transferred to a new dish to separate additional cells until it no longer adhered to the dish.

The complete culture medium consisted of Dulbecco's Modified Eagle's Medium/F12 (DMEM/F12, Corning, USA, cat: 10-092-CVRC) supplemented with 15% fetal bovine serum (FBS, Thermo Fisher Scientific, USA, cat: 10099141 C), 1% penicillin/streptomycin solution (100 U/mL, Solarbio, China, cat: P1400), 1% l-L-Glutamine solution (200 mM), 1% MEM Essential amino acid solution (NEAA) and 0.1% LIF.

Culture and passage of NCCs

When the cell density reached 70–80%, the culture medium was removed, and the cells were washed 1–2 times with PBS. A 0.25% trypsin solution was used for digestion, then digestion was stopped by adding the complete medium containing 10% serum. Cells were collected by centrifugation at 1000 rpm for 5 min, re-suspended in the complete medium, and transferred to a culture flask. Vigorous cells were collected using 0.25% trypsin, re-suspended in cryopreservation solution, and stored at − 80 ℃ overnight before transfer to liquid nitrogen for long-term storage. Cells passaged two to three times were used for further experiments.

Cellular immunofluorescence

After cleaning the cover glass with detergent, it was thoroughly washed clear water, followed by three washes with pure water, and soaked in 75% alcohol for 10 min. The cover glass was held with tweezers, heated above an alcohol lamp until dry and cooled. Temperature control was maintained to avoid overheating. The dried cover glass was placed in a 6-well plate, and the cell suspension containing $1–2 \times 10^4$ cells was dropped onto center. The plate was incubated at 37 °C and 5% CO_2, to allow cell adhesion and growth. After 3 h, 2 mL complete culture medium was slowly added along the well wall to prevent cells from detaching, and the plate was incubated overnight at 37 °C with 5% CO_2. The culture medium was discarded, and the wells were rinsed twice with PBS. Then, 1 mL of 4% paraformaldehyde (PFA) was added to each well for 10–15 min. The excess PFA was removed, the wells rinsed again with PBS, and 500 µL PBS was added for storage at 4 °C. After the final PBS wash, the slides were analyzed using an Andor Revolution-XD confocal microscope (Leica TCS SP8 X, Germany).

Plasmid construction and cell transfection

The *HOXD1* mRNA sequence (XM_004004562.5) was retrieved from NCBI (https://www.ncbi.nlm.nih.gov/), constructed on an ampicillin-resistant pcDNA3.1(+) plasmid and then transfected into competent cells. Monoclonal colonies were selected, cultured in Amp-resistant LB medium at 37 °C overnight, and observed for turbidity. Suitable cultures were chosen and submitted for sequencing (Shanghai Bioengineering Co., Ltd.). After confirming the correct gene sequence, large-scale cultures were prepared and bacterial plasmids were extracted. The primary NCCs were digested, seeded into a 6-well plate, and transiently transfected with either the *HOXD1* overexpression plasmid or an empty vector using Lipofectamine™ 3000 reagent (Thermo Fisher Scientific, Waltham, USA, cat: L3000015) for 24 h. The appropriate volumes of Lipo3000™ transfection reagent and plasmid mixture were added to each well, gently mixed, and incubated at 37 °C with 5% CO_2 for 48 h. The NCCs were then digested and collected into 1.5 mL tubes for further experiments.

Scratch test

Cells were seeded in a six-well plate and cultured until reached 90% confluent. Three straight lines were drawn with a sterile pipette tip, and floating cells were washed away with PBS. Unscratched cells were then cultured in a fresh complete medium. The blank gap was observed using a low-power phase-contrast microscope (Olympus, Japan). After 24 h, the blank gap was recorded and analyzed. The cell migration rate was calculated using formula:

migration rate (scratch distance at 0 h-scratch distance at 24 h)/scratch distance at 0 h. Images of the scratches were captured at 0, 6, 12, and 24 h using an Olympus inverted microscope at 100× magnification. The scratch width was analyzed with Olympus CellSens Dimension software (Olympus, Japan).

Cell counting kit-8 assay

Cell proliferation was assessed by a CCK-8 kit (Beyotime, China, cat: C0038) to compare differences between control and experimental groups. NCCs were cultured in 96-well plates, transfected with plasmid, and samples were collected at 0, 12, 24, 36, and 48 h. Then, 10 μL of CCK-8 reagent was added to each well, followed by incubator for 1–2 h. Absorbance was measured at 450 nm using a BioTek enzyme-labeled instrument (SynergyH1). The cell proliferation state was determined based on changes in absorbance.

Cell-cycle assay

Cell cycle and apoptosis were examined using the propidium iodide (PI) kit (BioFroxx, Germany, cat: 25535-16-4) and Annexin V-fluorescein isothiocyanate/PI double staining kit (Annexin V-FITC, BB-4101, BestBio) by flow cytometry (Becton Dickson Immunocytometry-Systems, San Jose, CA, USA), respectively. NCCs were seeded to 12-well plates containing cell slides and incubated in the complete medium. Cells were stained with propidium iodide (50 μg/mL $^{-1}$), and flow cytometry was used to detect the cell-cycle phase of control and *Hoxd1* siRNA-transfected cell. Experiments were performed according to the kit's instructions and repeated in triplicate.

RNA isolation, reverse transcription, and real-time PCR

Cells were harvested, and total RNA was isolated using TRIzol reagent (Takara, Japan, cat: 9109), following the manufacturer's protocol. RNA was purified by removing genomic DNA with a DNase I, RNase-free kit (Fermentas, Glen Burnie, MD, USA). One microgram of total RNA from each group (control and *HOXD1* siRNAs) was used for cDNA synthesis with the HiScript II Select qRT SuperMix II (Vazyme Biotech, Nanjing China, cat: R232-01), following the manufacturer's protocol. qPCR was performed on the CFX96 TouchTM Real-Time PCR Detection System (Bio-Rad) using SYBR Green (Roche). All samples were run in triplicate in 96-well plates, with each well containing 1.0 μL cDNA diluted 1:20, for a total reaction volume of 10 μL. Reactions were carried out at 95 °C for 1 min, followed by 40 cycles of 10 s at 95 °C, 10 s at 60 °C, and 30 s at 72 °C, then a final step of 5 min at 72 °C. The real-time PCR primers are listed in Table 1. For data analysis, the $2^{-\Delta\Delta CT}$ method was used for the analysis of the gene expression data and the expression was estimated in fold change for a glyceraldehyde-3-phosphate dehydrogenase (GAPDH) gene[19].

Western blotting (WB)

NCCs were seeded in six-well plates and incubated for 12 h in a complete culture medium. After washing the cells three times with PBS, the cells were lysed with pre-chilled radioimmunoprecipitation assay (RIPA) buffer containing protease and phosphatase inhibitors. The supernatant was collected for WB. Total protein concentration was measured using the BCA protein assay kit (Elabscience Biotechnology, Wuhan, China, cat: CB24808345). Proteins were separated by SDS-PAGE and transferred to a PVDF membrane, which was then blocked with 5% skim milk powder. The membrane was incubated in 5% goat serum for 60 min, followed by overnight incubation at 4 °C with antibodies against GADPH (1:10000), Vimentin (1:10000), α-SMA (1:5000), E-cadherin (1:5000), TGFBR1(1:5000), Smad4 (1:2000), β-catenin (1:2000), and Wnt2 (1:500). After washing with Tris-buffered saline cotaiining Tween 20 (TBST), the membrane was incubated with HRP-conjugated goat anti-rabbit or anti-mouse IgG secondary antibodies for 60 min at 37 °C. GAPDH served as an internal standard. Proteins on the membrane were then detected using the ECL kit (Kalang, Shanghai, China, cat: KL-X123) and imaging system (Bio-Rad).

Transcriptome analysis

Cultured NCCs were transfected with the *HOXD1* plasmid or control ($N = 3$) in the complete culture medium. Cells were washed three times with PBS, and total RNA was extracted using TRIZOL (Takara, Japan, cat: 9109). After confirming RNA integrity, library construction, and Illumina sequencing were performed on the BGI DNBSEQ high-throughput platform. Raw data were filtered by FastP (version: 0.21.0) tool (https://github.com/OpenGene/fastp) to obtain high-quality clean data. The FastQC (version: 0.11.9) tool was used to perform the quality control of raw reads (Phred score > 20, https://www.bioinformatics.babraham.ac.uk/projects/fastqc). The filtered RNA-seq reads were aligned to the C57BL6 mouse reference genome (https://github.com/alexdobin/STAR) to obtain comprehensive functional information for new transcripts and annotated in seven databases, including Nr, Pfam, Uniprot, KEGG, GO, KOG/COG, and PATHWAY. Differential expression analysis was conducted using DESeq2 software (version: 1.26.0), with gene screening criteria of absolute fold-change ≥ 2 and padj ≤ 0.05. The differential expressed genes were re-enriched in the GO and KEGG pathway databases. A hypergeometric test was used for statistical analysis, and cluster Profiler software (version: 3.14.3) was employed for enrichment analysis. The adjusted *p*-value (*p* adjust) was applied for multiple hypothesis testing, within the range of [0,1]. Two-dimensional PCA analysis was used to visualize the scatter plot with principal component 1(PC1) and principal component 2 (PC2) as axes, with each point representing a sample. Greater distances between PC1 and PC2 on the scatter plot indicated larger differences in gene expression patterns between samples.

Verification of differential expressed genes (DEGs)

Ten DEGs were randomly selected, and specific primers were designed on the NCBI website (Table 1). A total of 1000 ng of RNA was reverse transcribed into cDNA using a reverse transcription reagent (Takara, Japan,

Gene name	Accession number	Primer sequences (5′–3′)	Tm (°C)	Product length (bp)
GAPDH	NC_000072.7	F: AGGTCGGTGTGAACGGATTTG	60	123
		R: TGTAGACCATGTAGTTGAGGTCA		
HOXD1	XM_004004562.5	F: ACGAATCGAGATCGCCAACA	60	186
		R: CTTCCAGGGTTCTTTCCGCT		
TGF- β	NC_000068.8	F: ACAGCAAAGATAACAAACTCCACG	60	197
		R: CTTCTCTGTGGAGCTGAAGCA		
TGF-BR	NC_000070.7	F: TCCTTCAAACGCGCTGACAT	60	200
		R: CAGCTCTGCCATCTGTTTGG		
Samd3	NC_000076.7	F: TGTCAACCAGGGCTTTGAGG	60	179
		R: CCATCTGGGTGAGGACCTTG		
Samd4	NC_000080.7	F: GGGAGGAGATCGCTTTTGCT	60	98
		R: CCAACTGCACTCCTTTGCCT		
Wnt2	NC_000072.7	F: GGCCTGTAGCCAAGGAGAAT	60	172
		R: GGCATCCTTGCCTTTCCTCT		
β-catenin	NC_000075.7	F: CTGGGACTCTGCACAACCTT	60	134
		R: CAGTGTCGTGATGGCGTAGA		
Vimentin	NC_000068.8	F: GCTTCTCTGGCACGTCTTGA	60	160
		R: TGAGGTCAGGCTTGGAAACG		
E-cadherin	NC_000074.7	F: CAGCCGGTCTTTGAGGGATT	60	128
		R: TGACGATGGTGTAGGCGATG		
α-SMA	NC_000085.7	F: GCTACGAACTGCCTGACGG	60	127
		R: GCTGTTATAGGTGGTTTCGTGG		
CXCL2	NC_000071.7	F: CATAGCCACTCTCAAGGGCG	60	103
		R: TCAGTTAGCCTTGCCTTTGTTC		
CXCL3	NC_000071.7	F: TGCCTGAACACCCTACCAAG	60	88
		R: CTTCTGTCTGGGTGCAGTGG		
IL-1 A	NC_000068.8	F: ACGTCAAGCAACGGGAAGAT	60	124
		R: AAGGTGCTGATCTGGGTTGG		
Mmp3	NC_000075.7	F: TTCTGGGCTATACGAGGGCA	60	84
		R: CTTCTTCACGGTTGCAGGGA		
Chi3l1	NC_000067.7	F: GGAGAAGAAGCTGGCAGGAG	60	105
		R: TCCTTGATGGCGTTGGTGAG		
Tgfbi	NC_000079.7	F: TCAAAGATGGTGTCCCTCGC	60	139
		R: AAGACTCGCAGCTTTTTGCC		
Prelp	NC_000067.7	F: TTGCCCCAACAACCTAGTGG	60	120
		R: ATGAGGTCCAGTGGGATGGG		
Ogn	NC_000079.7	F: CGACCTGGAATCTGTGCCTC	60	131
		R: TTCGCTCCCGAATGTAACGA		
Megf6	NC_000070.7	F: CTGTGATTGTGGGGGTGGG	60	124
		R: GGGTGCTGGTCTGATAGAGG		
Adamts5	NC_000082.7	F: TGTTGCTGCTACTGCTGCT	60	91
		R: TGCCTGGTTTTATCCTGGGC		

Table 1. Gene name, accession number, primer sequences, amplicon sizes, and optimal annealing temperatures.

cat: RR037A). qRT-PCR was performed to analyze the relative expression levels of DEGs with a TB Green chimeric fluorescence assay (Takara, Japan, cat: RR820A). Ubiquitously expressed prefoldin-like chaperone (UXT) and ribosomal protein S9 (RPS9) were used as double internal references, and the $2^{-\Delta\Delta ct}$ method was applied to calculate relative mRNA levels[19]. The primer sequences of the detected gene are listed in Table 1. Data were analyzed using SPSS19.0 software for one-way ANOVA, and log2 Fold Change was used to convert fold differences. GraphPad Prism 8 was used for plotting data based on gene expression and transcriptome results.

Results

Isolation and identification of NCCs

The first branchial arch tissue was isolated from mouse embryo and cultured in a 5% CO_2 incubator at 37 °C for 12 h. Several spindle cells migrated around the tissue block. After 48 h, the tissue block was removed (Fig. 1A), and the culture medium was changed. Cells were cultured for an additional 48 h. Cells grew in the blank area

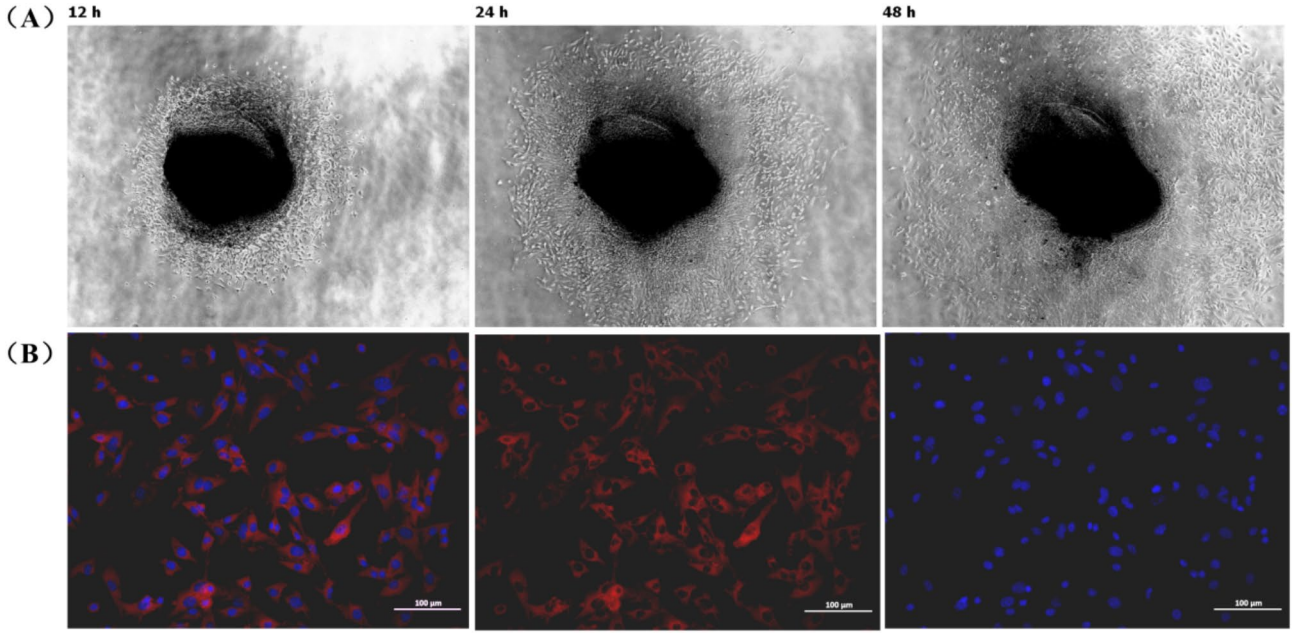

Fig. 1. Cell migration and immunofluorescence. (**A**) Cell migration at 12, 24, and 48 h after tissue block adherence (×40). (**B**) Immunofluorescence of SOX10 in neural crest cells (×200).

where the tissue block was originally placed (Fig. 2A), and those with good growth status were selected for cryopreservation. Mouse NCCs were isolated, digested with 0.25% trypsin solution, seeded evenly into cell culture bottles, and cultured in a 5% CO_2 incubator at 37 °C for 24 h. Microscope observation showed that the cells grew evenly, adhered to the wall, and were spindle-shaped, consistent with the physiological characteristics of nerve cells (Fig. 2B). Cell climbing slices were prepared and identified by SOX10 gene immunofluorescence. The results demonstrated strong SOX10 expression in over 95% of the cells (Fig. 1B), confirming the isolated cells as mouse NCCs.

Vector construction and cell transfection

The recombinant pcDNA3.1-HOXD1 vector was successfully constructed using pcDNA3.1 (Fig. 3A). Sequencing results confirmed the correct overexpression vector (Fig. 3B), suitable for further experiments. The *HOXD1* gene overexpression vector was transfected into mouse neural crest cells. Quantitative analysis showed that *HOXD1* expression in the treatment group was significantly higher than in the control group ($P < 0.001$), confirming successful transfection (Fig. 4A).

Scarification test

Cell migration was assessed using the cell scratch assay. After transfection with control or *HOXD1* overexpression plasmid, cells were scratched and photographed at 0, 6, 12, and 24 h at marking locations (Fig. 4B). The scratch test confirmed that *HOXD1* overexpression significantly improved migration efficiency at 6 h and 24 h ($P < 0.05$, Fig. 4C). Although migration efficiency increased at 12 h, the change was not significant ($P > 0.05$, Fig. 4C). The results indicated that *HOXD1* gene overexpression significantly inhibited the migration ability of neural crest cells in culture.

CCK-8 and cell periodic flow assay

After transfecting of the control and *HOXD1* overexpression plasmid, CCK-8 results showed that *HOXD1* overexpression did not significantly affect NCC proliferation compared with the control group ($P > 0.05$, Fig. 5). After treating the mouse NCCs with *HOXD1* overexpression for 48 h, the cell cycle was analyzed by flow cytometry (Fig. 6). The results indicated no significant differences in the G1, G2, or S phases compared to the control ($P > 0.05$), and the proportion of cells in the G1/G2 phase also showed no significantly changes ($P > 0.05$). Thus, *HOXD1* overexpression did not affect the cell cycle of mice NCCs.

Effect on EMT marker gene mRNA level and protein expression

The expression level of EMT marker genes were measured by qRT-PCR, and EMT-related proteins expression was confirmed by WB. The results indicated that *HOXD1* expression in NCCs was significantly higher than in the NC group ($P < 0.01$, Fig. 4A). *HOXD1* overexpression also significantly increased the expression of mesenchymal marker genes, such as *Vimentin* and *E-cadherin* ($P < 0.05$), while α-SMA expression did not increase significantly ($P > 0.05$, Fig. 7A). Protein analysis showed that *E-cadherin* protein levels significantly increased ($P < 0.01$), but *Vimentin* and *α-SMA* protein levels did not change significantly ($P > 0.05$, Fig. 7B,C). These suggest that *HOXD1* overexpression may induce EMT in NCCs by regulating *Vimentin* and *E-cadherin* expression.

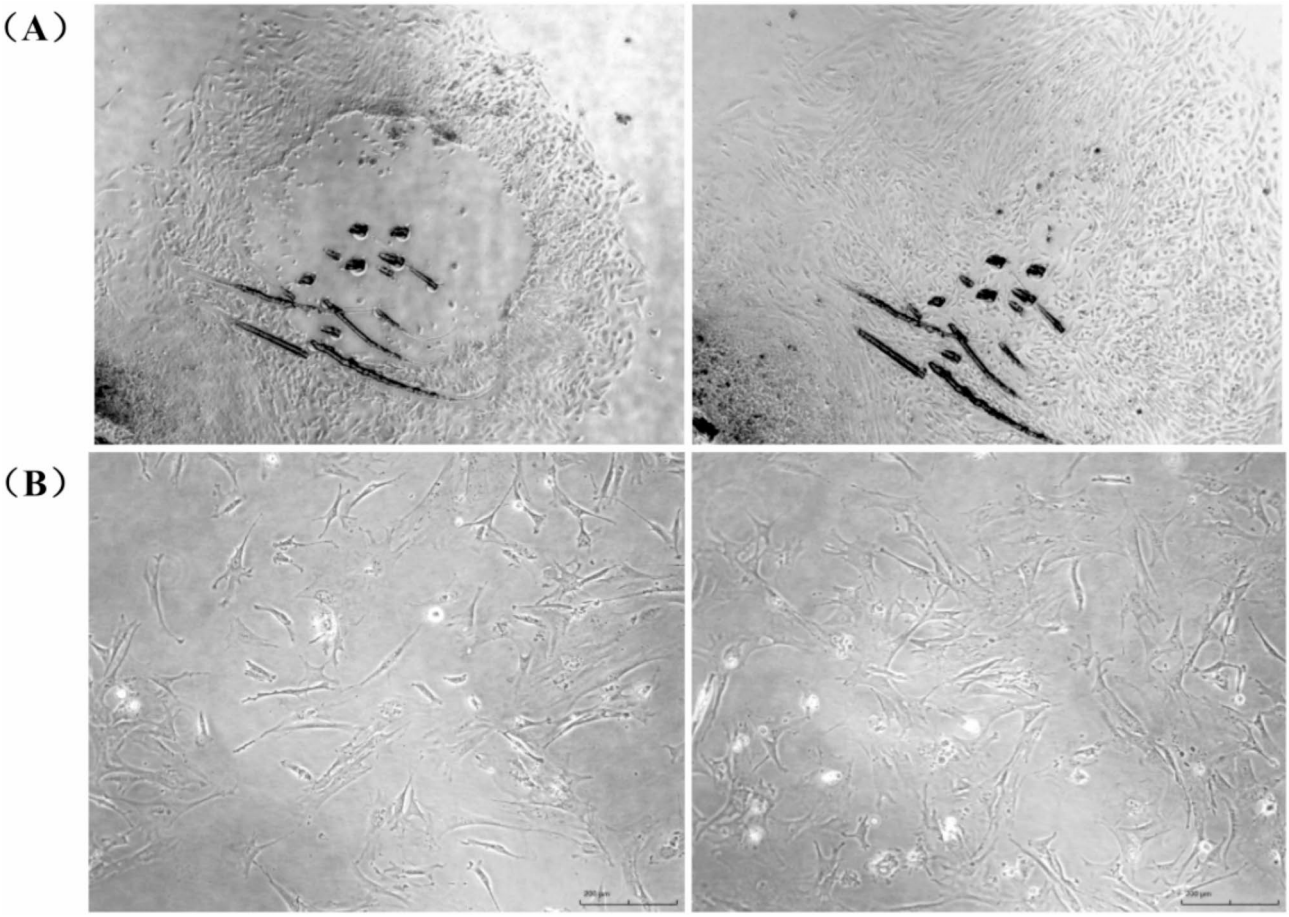

Fig. 2. Morphological characteristics of mouse neural crest primary cells. (**A**) Cell growth at 0, 24 h after tissue block removal (×40). (**B**) Morphology of mouse neural crest primary cells (×40).

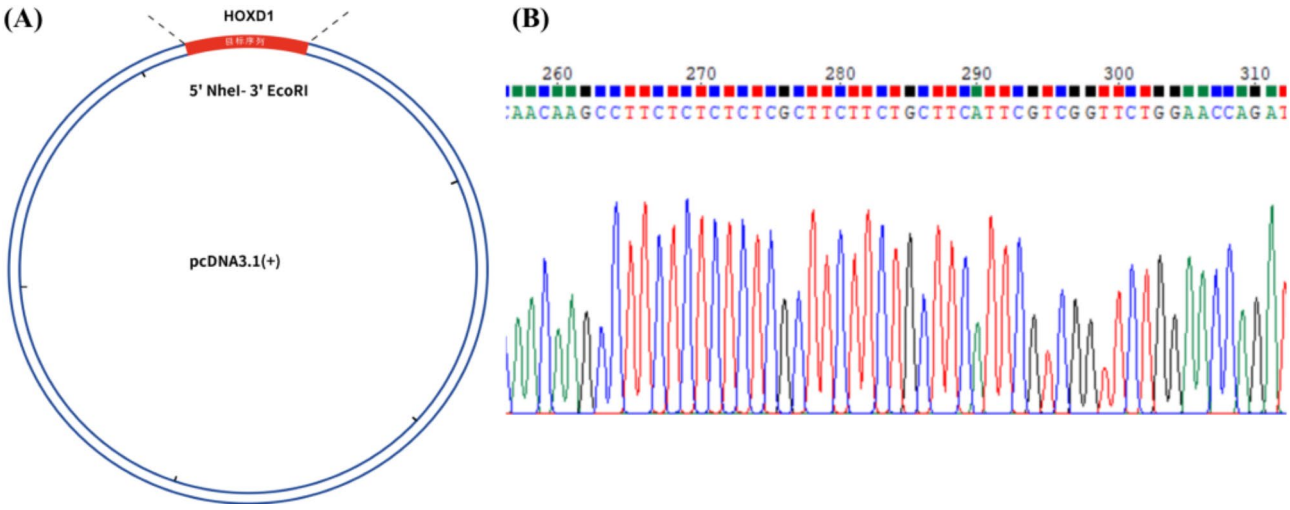

Fig. 3. Schematic representation of sheep *HOXD1* gene overexpression vector. (**A**) Schematic diagram of recombinant plasmid pcDNA3.1-HOXD1. (**B**) Fragment diagram of pcDNA3.1-HOXD1 sequencing.

Expression of key genes in Wnt and TGF signaling pathways

To investigate the possible signaling pathways mediated by *HOXD1* in NCCs, the expression levels of key Wnt and TGF pathway genes were measured by qRT-PCR and WB (Fig. 8). Figure 8B,D show that *HOXD1*overexpression significantly increased Wnt2 and β-catenin mRNA expression in the Wnt pathway ($P<0.05$), but had no

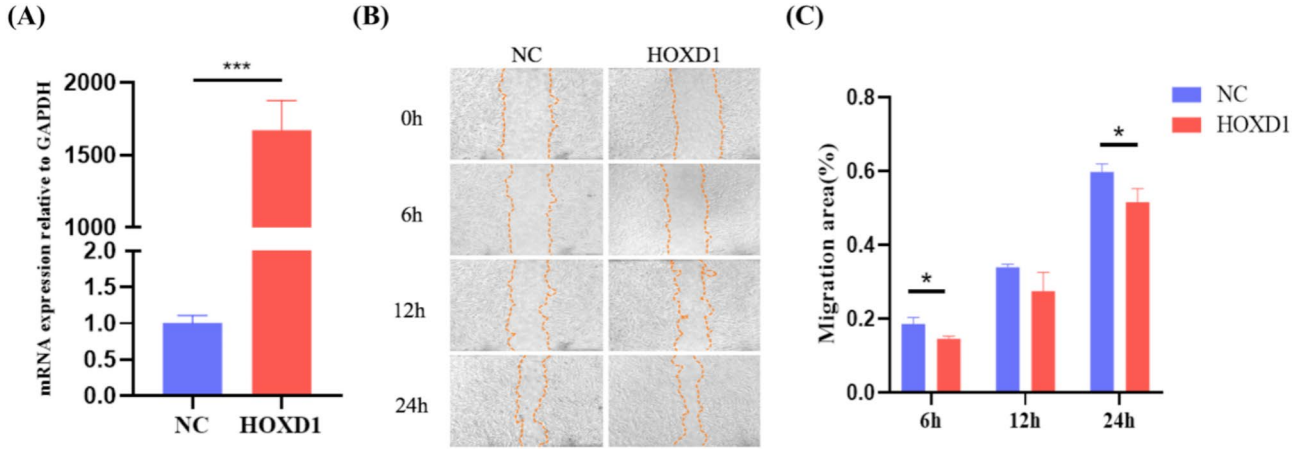

Fig. 4. *HOXD1* gene overexpression and the migration effect in mouse neural crest cells. (**A**) Overexpression efficiency of *HOXD1*. (**B**) Cell scratch plot. (**C**) Cell scratch quantification results.

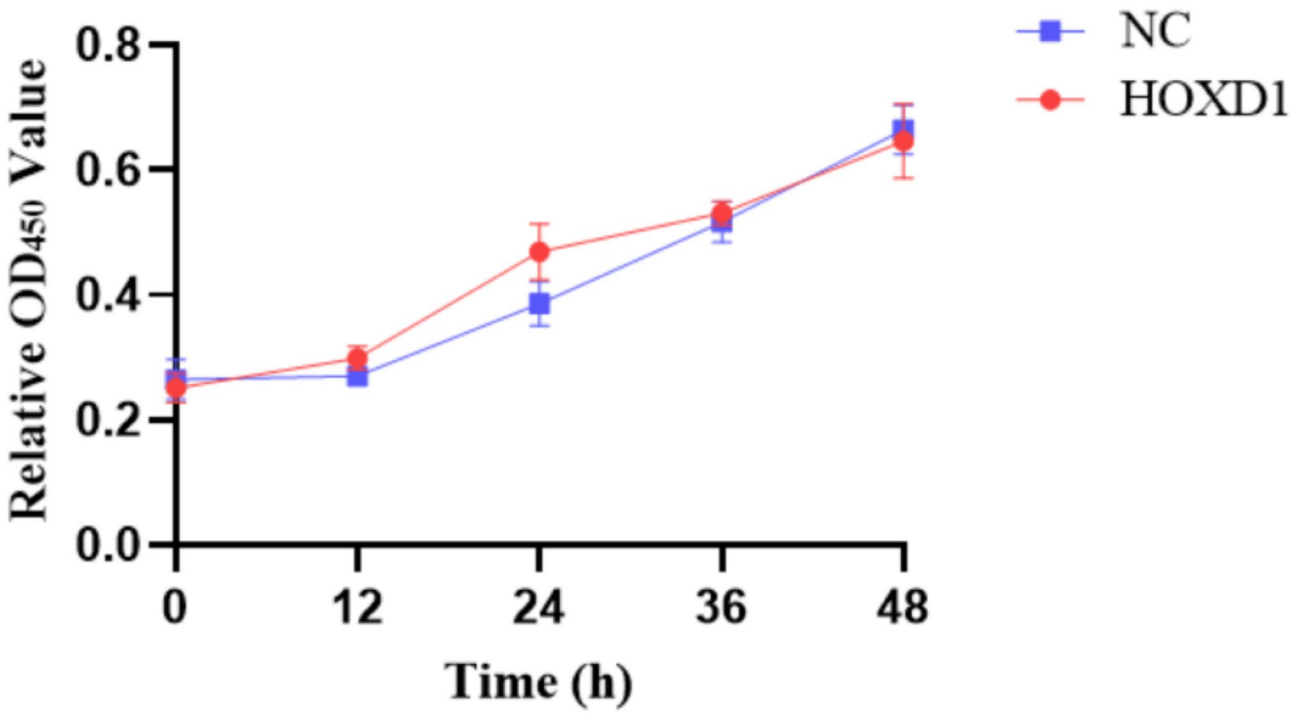

Fig. 5. Viability of mouse neural crest cells at 12, 24, 36, and 48 h after *HOXD1* overexpression.

significant effect on *TGF-β*, *TGF-BR*, *Smad3*, or *Smad4* mRNA levels in the TGF pathway ($P > 0.05$). The results suggest that *HOXD1* primarily regulates Wnt signaling rather than TGF-β signaling. Figure 8A,C that protein expression of TGF-BR, Wnt2, and β-catenin was upregulated, wherease Smad4 protein levels were downregulated. WB analysis confirmed that *HOXD1*overexpression increased Wnt2, β-catenin, and TGF-BR protein levels in NCCs, while significantly reducing Smad4 protein levels. These findings suggest that *HOXD1* may inhibit NCC proliferation by modulating Wnt signaling.

Analysis of *HOXD1* co-expressed genes in NCCs

To investigate the functions mediated by *HOXD1* in NCCs, we analyzed its co-expressed genes using transcriptomic sequencing data. Cultured NCCs were transfected with the *HOXD1* plasmid or control in the complete culture medium. A total of six cultured NCCs libraries were constructed and used for sequencing via high-throughput. In total, 355.69 Gb data were generated in both transfected with the *HOXD1* and control in NCCs. The details of the total data, total number of reads, aligned reads, and unaligned reads aliments for all the samples were mentioned in Table S1. Differential gene analysis results showed that the closely related genes

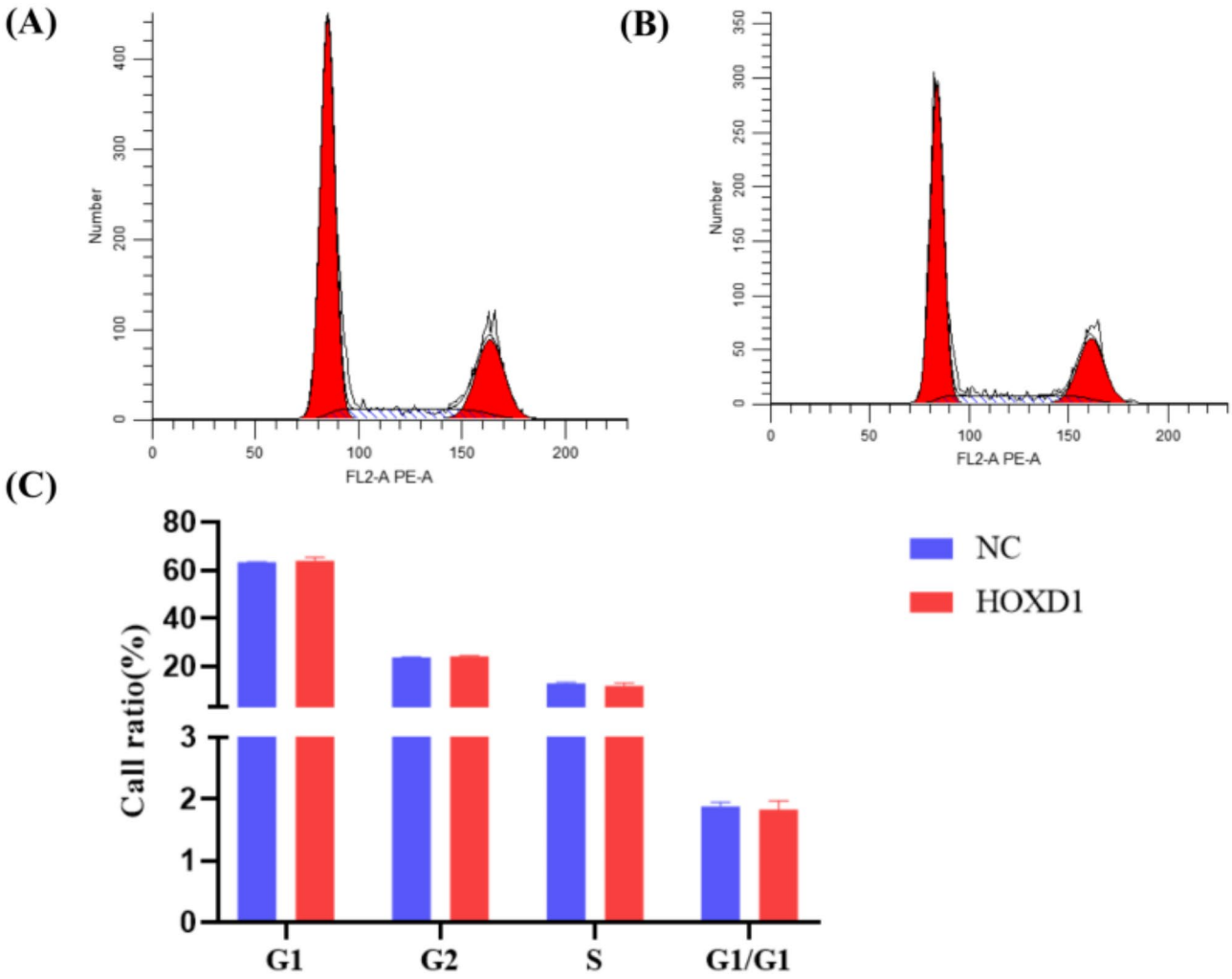

Fig. 6. Cycle distribution of mouse neural crest cells. (**A**) Overexpression of *HOXD1* gene cell cycle. (**B**) Control cell cycle. (**C**) Statistical plot of cell cycle in experimental and control groups.

of *HOXD1* are displayed in a volcano plot (Fig. 9A). PCA showed clear differences between the control and experimental groups, and the biological repeatability within group was reasonable (Fig. 9B). In total, 59 genes were significantly down-regulated and 80 were significantly up-regulated in mouse NCCs compared to controls (Fig. 9C, Table S2).

To explore the functions of DEGs, GO enrichment, GO annotation, and KEGG enrichment were performed on the NCBI website (Fig. 10). KEGG enrichment identified the top five signaling pathways as IL-17 signaling, TNF signaling, whooping cough, cytokine-receptor interaction, and legionellosis (Table 2). The signaling pathway with the most enriched differential genes was cytokine-receptor interaction (Fig. 10A). GO enrichment indicated the top five categories: CXCR chemokine receptor binding, platelet α granule, growth factor activity, cytokine activity, and cell response to lipopolysaccharide (Table 2; Fig. 10B). GO annotation revealed enrichment in molecular function (MF), biological process (BP), and cellular component (CC) categories. Molecular functions were mainly associated with cytokine and receptor activities (receptor ligand activity, signal receptor activator activity) (Fig. 10C). In the biological processes, enrichment was noted for cell response (e, g., to lipopolysaccharide, bacterial molecules.), while cellular components were primarily linked to the extracellular matrix (extracellular region, and intercellular space). Both enrichment and annotation analyses focused on the extracellular matrix. NCBI gene annotation of DEGs outside KEGG pathways indicated associations with bone differentiation and changes in extracellular components. Most proteins expressed by these genes were located in the extracellular matrix, including *Ogn*, *Aspn*, *Fbn2*, *Tgfbi*, *Adamtsl1*, *Bmp4*, *Megf6*, *Lrrc17*, *Serpinb7*, and *Prg4* (Table S2).

As shown in Fig. S2, validation of DEGs revealed that five genes (*CXCL2*, *CXCL3*, *LI1a*, *Mmp3*, and Chi3l1) were down-regulated, while five genes (*Tgfbi*, *Prelp*, *Ogn*, *Adamts5*, and *Megf6*) were up-regulated. qRT-PCR results were consistent with RNA sequencing, confirms the reliability of the transcriptome data. KEGG enrichment showed that the overexpression of *HOXD1* in mouse NCCs led to DEGs concentrated in muktiple cytokine-receptor interaction pathways (Fig. S3, The image is obtained from KEGG website (map04060), http://www.kegg.jp/kegg/kegg1.html)[20–22]. Analysis of DEGs in these pathways revealed significant decreases in CXC

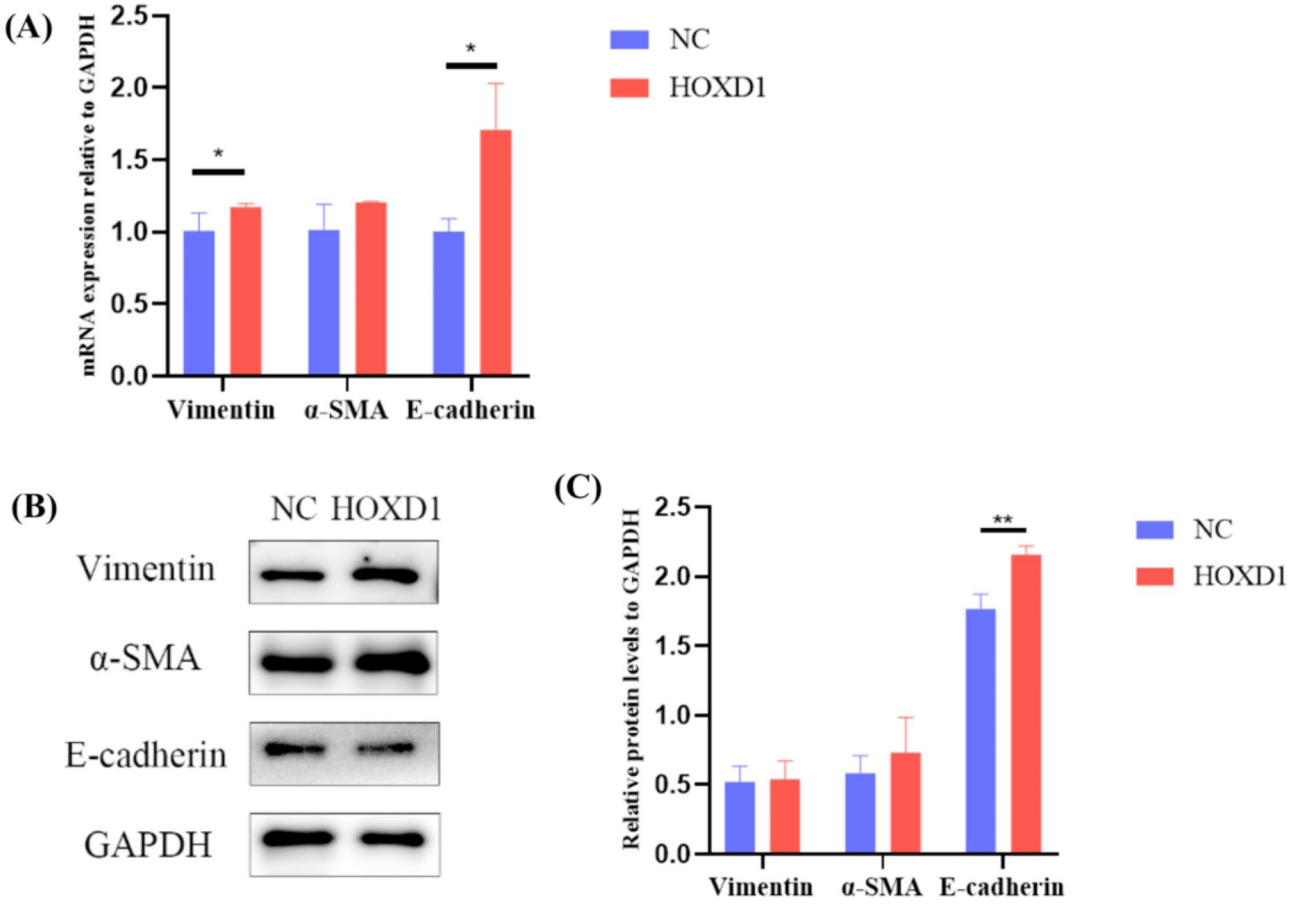

Fig. 7. Expression of each gene after *HOXD1* overexpression in mouse neural crest cells. (**A**) mRNA expression of EMT marker genes. (**B**) Protein expression of EMT marker genes. (**C**) Protein profile of EMT marker genes.

family chemokines *(CXCL1*, *CXCL2*, *CXCL3*, *CXCL7*, *CXCL10*), and type I cytokines (*CSF2*, *PRL*, *CSF3*, IL12, *LIF*, *IL1A*, *IL1B)*.

Discussion

The neural crest cells were isolated and identified

The multi-horned traits in sheep is a complex phenotype regulated by polygenes. Genetic studies of the polycerate traits in sheep have been reported in many literatures[2–7,14]. However, the mechanism behind multi-horned traits development and growth remains unclear. To study the role of *HOXD1* in sheep horn development and growth, we considered NCCs which have shown promise in previous research on tooth development and dental tissue/tooth organ regeneration[23]. Gene expression profiles of antlers resemble those of sheep and are derived from tissues such as nerves, bones, and skin. It is well-known that the ruminant horns originate from NCCs[24]. These pluripotent cells arise at the boundaries of the developing nervous system and surface ectoderm, differentiating into a various cell types that contribute to multiple organs and systems[25]. Antler blastema progenitor cells (ABPCs) have been identified as key chondrocytes in antler regeneration through single-cell sequencing, ABPCs are likely derived from resting stem cells (PMC2) in the antler area periosteum before regeneration[26]. The antler area periosteum is thought to be an embryonic tissue retained after birth[27]. This periosteum is considered an embryonic tissue retained after birth. Some studies suggest that craniofacial NCCs retain pluripotent stem cells in the antler zone periosteum during embryonic development, leading to similar hypotheses by various researchers[24]. Therefore, to study the process of sheep horn development, the selection and separation of mouse NCCs is the primary work. In current study, we selected mouse NCCs as our research model and successfully isolated them from embryonic first branchial arch tissue blocks of C57BL/6 pregnant mice. After 12 h of incubation, a certain number of spindle-shaped cells migrated around the tissue blocks (Fig. 1A). By 48 h, cells had adhered to the culture surface, exhibiting spindle shapes consistent with neural cell characteristics (Fig. 2A). Immunofluorescent staining showed that *SOX10* was expressed in over 95% of the cells (Figs. 1B and 2B), confirming their identification as mouse NCCs for subsequent studies.

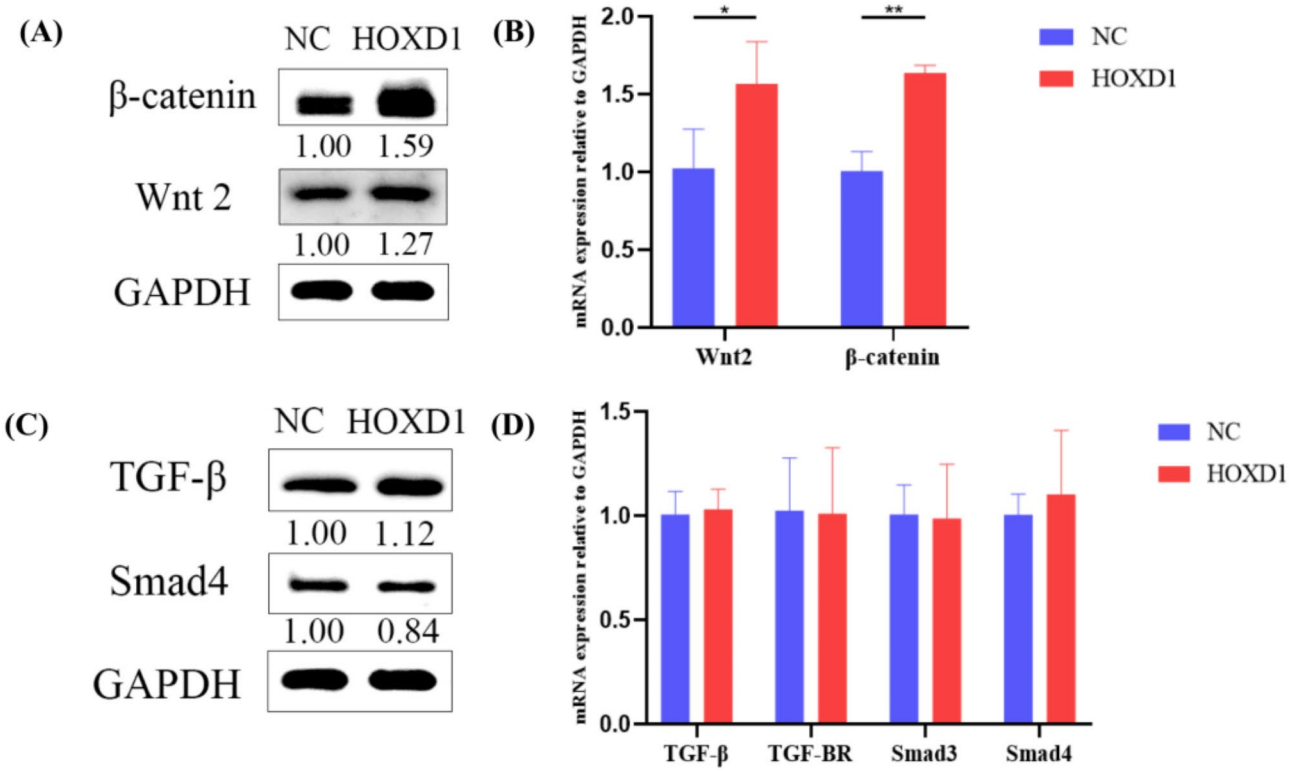

Fig. 8. Expression of key genes in Wnt and TGF signaling pathways. (**A**) Protein expression of key genes in Wnt signaling pathway. (**B**) mRNA expression of key genes in Wnt signaling pathway. (**C**) Protein expression of key genes in TGF signaling pathway. (**D**) mRNA expression of key genes in TGF signaling pathway.

The regulatory mechanism of *Hox* gene clusters in embryonic development

Hox gene clusters are involved the control of many key processes in the development of metazoans, such as the determination of tissue identity, the establishment of the anterior-posterior axis, segmentation, and the formation of appendages and limbs[28]. *Hox* gene clusters have many characteristics, the most distinctive of which is that they control development of the embryo's body along the head-to-tail axis, followed by spatial and temporal collinearities[29], and specific cascade effects[30]. *HOXD1* is the first gene in the *HOXD* gene families of the *Hox* gene cluster[29]. The gene expression levels in the *Hox* gene cluster are related to the quantity and size of the phenotype[31]. Studies interfering with the expression level of the 11th, 12th, and 13th groups of genes in *HOXD* and *HOXA* can control the size and number of mouse toes[9]. The same four *Hox* gene expression quantities are also related to the formation of the external genitalia[32]. The *Hox* gene Ubx can regulate the morphology of the legs in Drosila, especially by inhibiting the formation of non-sensory microchaeta or setae on the second and third legs of different species of Drosophila[33]. Different Ubx expression patterns result in different setae distribution patterns, and this pattern is affected by the Ubx expression level, which requires a high level Ubx expression to effectively inhibit, and Ubx can also regulate the length of the legs according to its expression level in the water sheath[34]. The Hox may be through affecting the positioning of enhancers, thereby appropriately regulating the transcription of genes by other transcription factors in specific structural domains of the nucleus[31]. In our experiments, we found that the *HOXD1* gene was overexpressed in neural crest cells, and the different genes were mainly enriched in the interaction of cytokine-cytokine receptors, with 12 genes in the *CXC* family of chemokines. How *Hox* gene clusters regulate other genes? *Hox* gene clusters may have characteristics of pioneer transcription factors[8], which can further regulate the chromatin state by binding to low-open chromatin[35], and the difficulty of combination is related to the number of regulatory elements on the transcription factor[8]. The same conclusion was also drawn in the study of mammals[36]. These results provided experimental references for the study of *HOXD1* function in the polycerate growth and development of sheep.

HOXD1 induced EMT via Wnt signaling pathway

HOXD1 4 bp deletion has been found to cause different horn region sizes in fetuses with various genotypes in polycerate sheep. The horn size in homozygous deletions is larger than in heterozygous deletions, and both are larger than that in homozygous wild-type, indicating that the angular basis size is related to the *HOXD1* gene expression[7]. And it has been verified in Chinese sheep populations, and the 4dp deletion of *HOXD1* was only found in the four-horned of Sishui fur sheep breed[14]. To investigate the role of *HOXD1* in the migratory ability and viability of mouse NCCs, we overexpressed *HOXD1* in these cells (Fig. 4A). CCK-8 and cell cycle assays showed that had no significant change in cell viability following *HOXD1* overexpressing (Figs. 5 and 6). In terms of cell migration, scratch test results indicated that the migration rate was significantly lower in the *HOXD1*-

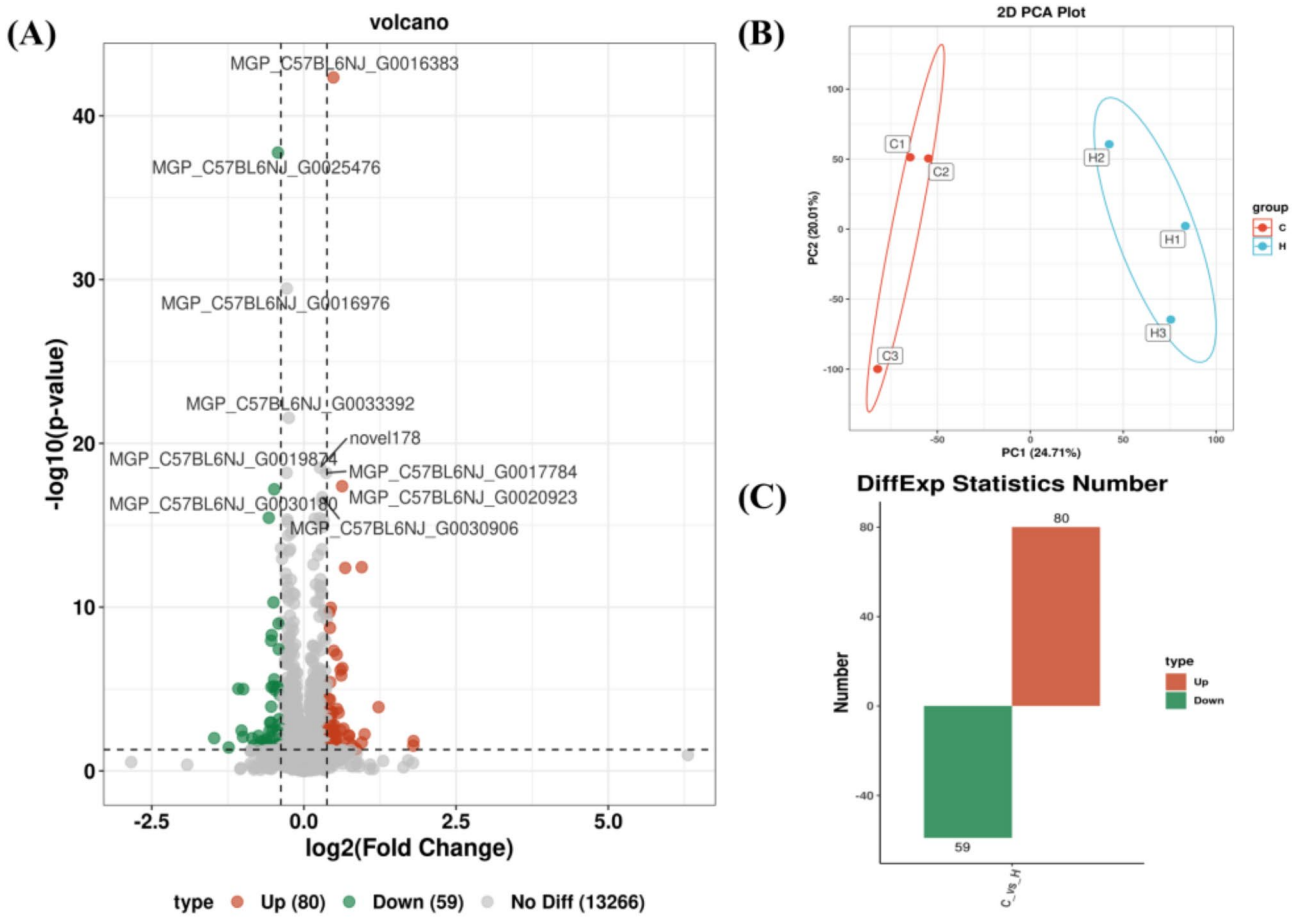

Fig. 9. Differential gene analysis of mouse neural crest cells after overexpression of *HOXD1* gene. (**A**) Volcano map of differential expressed genes. (**B**) Principal component analysis diagram. (**C**) Statistical map of differential expressed genes.

overexpressing group compared to the control group (Fig. 4B,C). Meanwhile, WB and qRT-PCR results showed that *HOXD1* overexpression up-regulated *E-cadherin*he expression, an EMT marker, but did not significantly affect of *Vimentin* expression or *α-SMA* expression (Fig. 7). Although EMT is often considered a transient process, recent advances in single-cell RNA sequencing have revealed multiple transitional EMT states along the epithelial to mesenchymal spectrum[37]. In studies on lung, ovarian, skin, and breast cancer, one prominent feature of EMT transitional cells is the co-expression of epithelial cell markers (*E-cadherin*, *Cytokeratin*) and mesenchymal markers or EMT-related genes (*E-cadherin*, *SNAIL1*)[38–41]. Our results indicated that *HOXD1* overexpression induced EMT changes in NCCs, keeping the cells in a transition EMT state and significantly reducing migration.

After *HOXD1*overexpression, we examined the key genes regulating the TGF and Wnt signaling pathways of EMT. The results showed that *HOXD1* had no significant effect on the TGF signaling pathway but significant up-regulated the Wnt signaling pathway (Fig. 8). Surprisingly, Wnt pathway activation did not result down-regulate *E-cadherin*. *E-cadherin* expression is influenced by multiple regulatory mechanisms, requiring regulatory factor to enter the nucleus[42]. Additionally, *HOXD1* activation inhibited cell proliferation and the cell cycle via the Wnt and TGF-β g pathways, suggesting a tumor suppressor role[11]. We hypothesized that *β-cadherin* might be blocked before entering the nucleus, or other pathways could regulate *E-cadherin* expression, thereby weakening the effect of the Wnt pathway. These findings suggest that *HOXD1* may inhibit NCC proliferation by modulating Wnt signaling rather than TGF-β signaling.

The CXC family may be a downstream regulator of the *HOXD1* gene

To explore the specific pathway through which the *HOXD1* gene affects NCCs, the transcriptome of mouse NCCs was analyzed 48 h after *HOXD1* overexpression. A total of 139 DEGs were identified, including 59 down-regulated genes and 80 significantly up-regulated genes (Fig. 9). KEGG enrichment analysis showed significant enrichment in cytokine-receptor interaction, with 12 down-regulated genes, mainly cytokine (Fig. 10A). The down-regulated genes belonged to the CXC family, including *CXCL1*, *CXCL2*, *CXCL3*, *CXCL7*, and *CXCL10*, with receptors *CXCR1*, *CXCR2*, and *CXCR3*. GO enrichment analysis indicated that these differential expressed genes were primarily associated with CXCR chemokine receptor binding, growth factor activity, and cytokine activity (Fig. 10B,C). The CXCR chemokine receptor binding function is mainly regulated by the ability of the

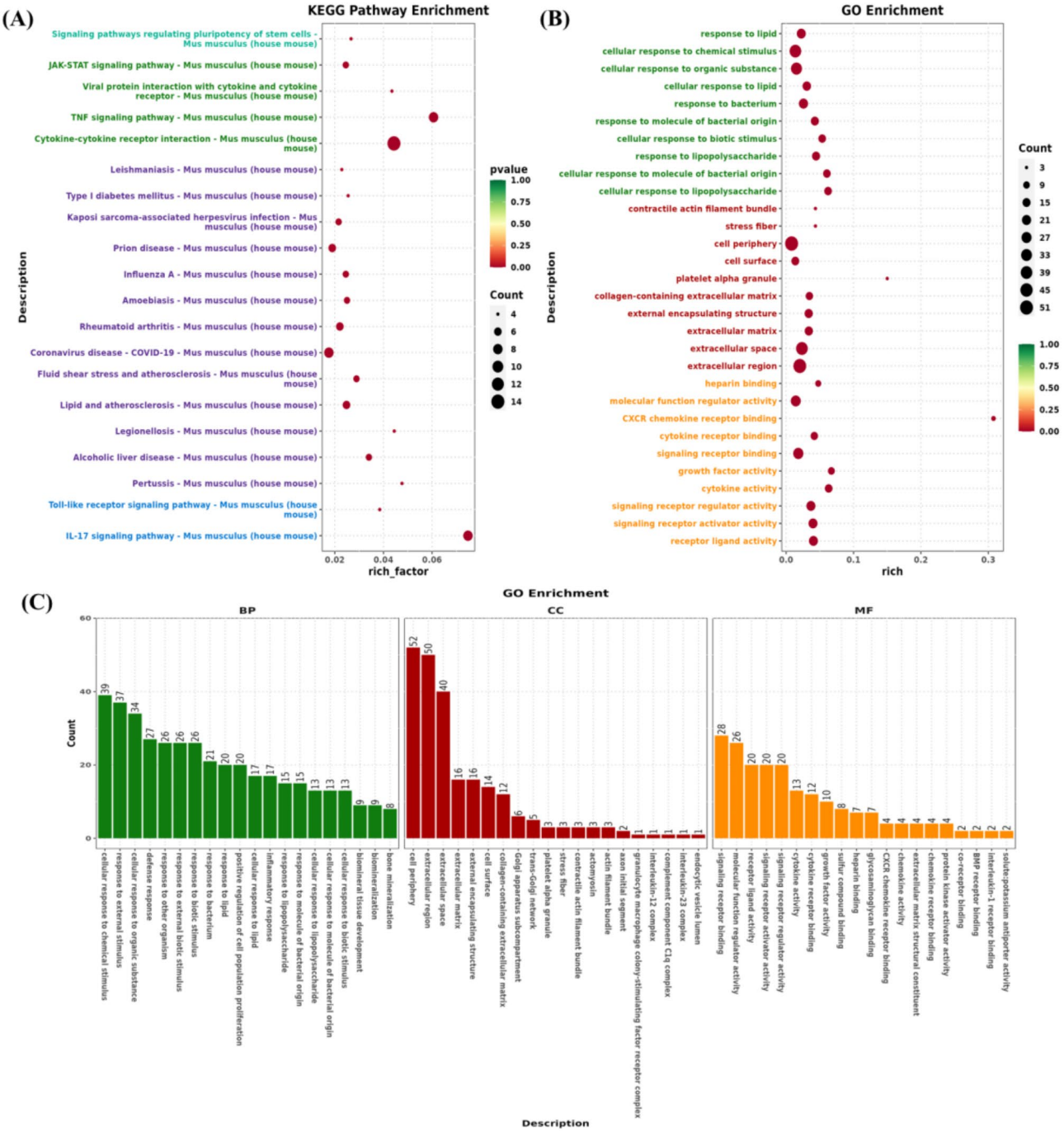

Fig. 10. Functional enrichment of differential expressed genes. (**A**) KEGG functional enrichment analysis. (**B**,**C**) GO functional enrichment analysis.

CXC family to bind to receptors, consistent with KEGG enrichment findings. Growth factors and cytokines are key components of the extracellular matrix. As a chemokine subfamily, the CXC family play crucial roles in cells development, influencing cell motility, localization, survival, and proliferation in both developing and adult tissues[43]. The CXC family also regulates cancer cell migration. For example, overexpression of *CXCR1* or *CXCR2* increases melanoma cell proliferation and invasion, while knockdown of CXCR1 and/or CXCR2 inhibits melanoma cell growth, motility, and vascularization[44,45]. In gastric cancer, CXC family cytokines (*CXCL1*, *CXCL2*, *CXCL3*, *CXCL5*, *CXCL8*) significantly change before and after treatment, CXC receptors also exhibit varying expression levels at different stages, serve as diagnostic markers for disease progression[46]. Generally, the ELR + CXCLs/CXCR1/2 signaling pathway promotes tumor progression, while the ELR-CXCLs/CXCR 3 ~ 7 signaling pathway mainly inhibits tumor[47]. Additionally, the ELR + CXCLs/CXCRs signaling axis activates MAPK, PI3K/AKT, β-catenin, STAT3, NF-Kb, and Ras pathways mediating tumor cell proliferation, metastasis, angiogenesis, and malignant transformation[46]. Transcriptome analysis revealed that *CXCL1*, *CXCL2*, *CXCL3*,

Category	Description	Second category	ID	*P*-value	Rich factor	Gene name
KEGG	IL-17 signaling pathway	Organismal systems	mmu04657	1.64×10^{-7}	0.075	*Cxc110*, *I11b*, *Cxc12*, *Len2*, *Mmp13*, *Cxc13*, *Csf2*, *Csf3*
	TNF signaling pathway	Environmental information processing	mmu04668	8.26×10^{-7}	0.061	*Cxc110*, *I11b*, *Cxc12*, *Lif*, *Cxc13*, *Csf2*, *Traf1*
	Pertussis	Human diseases	mmu05133	0.0014	0.048	*Illa*, *Il1b*, *C1qc*, *I112b*
	Cytokine–cytokine receptor interaction	Environmental information processing	mmu04060	2.20×10^{-9}	0.044	*Cxc110*, *Illa*, *Il1b*, *Cxc12*, *Lif*, *Cxc13*, *Ppbp*, *Csf2*, *Csf3*, *Il12b*, *Bmp2*
	Legionellosis	Human diseases	mmu05134	0.0018	0.044	*Il1b*, *Cxc12*, *Cxc13*, *Il12b*
GO	CXCR chemokine receptor binding	Cellular component	GO:0045236	8.71×10^{-7}	0.308	*Cxcl10*, *Cxcl2*, *Cxcl3*, *Ppbp*
	Platelet alpha granule	Molecular function	GO:0031091	0.0002	0.150	*Igf1*, *Ppbp*
	Growth factor activity	Molecular function	GO:0008083	2.29×10^{-8}	0.067	*Ogn*, *Igf1*, *Lif*, *Ptn*, *Bmp4*, *Gdf10*, *Csf2*, *Csf3*, *I112b*, *Bmp2*
	Cytokine activity	Biological porcess	GO:0005125	3.34×10^{-10}	0.063	*Illa*, *I11b*, *Lif*, *Bmp4*, *Gdf10*, *Csf2*, *Csf3*, *I112b*, *Bmp2*
	Cellular response to lipopolysaccharide	Biological porcess	GO:0071222	4.71×10^{-10}	0.062	*Cxc110*, *Illa*, *I11b*, *Cxc12*, *Mrc1*, *Cxc13*, *Cmpk2*, *Cd274*, *Tnip3*, *Ppbp*, *Csf3*, *Cd86*, *I112b*

Table 2. Details information of the top 5 KEGG pathways and GO terms.

CXCL7, and *CXCL10* genes in the CXC family were down-regulated. However, the regulatory mechanisms linking the down-regulation of these genes, *HOXD1* overexpression in neural crest cells and cells migration inhibition require further investigation.

We also annotated the DEGs outside the KEGG signaling pathway and found that most DEGs were located in the extracellular matrix. Genes related to the extracellular matrix include *Serpinb7*, *Ogn*, *Tgfbi*, and *Adamtsl1*, while genes linked to cell migration include *Cdsn*, *Limch1*, and *Mmp3*. Among these, the *Mmp3* gene belongs to the matrix metalloproteinases family, a group of zinc-dependent proteolytic enzyme that degrade various extracellular matrix protein and play key roles in processes, such as embryogenesis, tissue remodeling, wound healing, angiogenesis, and cancer[48]. The *Mmp3* gene was significantly down-regulated consistent with observed inhibition of neural crest cells migration in the scratch test. Other DEGs are associated osteocytes differentiation and neurons growth, including *Aspn*, *Ednra*, *Fbn2*, *Tifab*, *Bmp4*, *Lrrc17*, and *Bmp2*. *Bmp4* and *Bmp2* are bone morphogenetic proteins, part of a highly conserved signaling pathway across species, which plays an important role in skeletal development[49]. During embryonic development, abnormal expression or mutation of these protein in cranial neural crest cells can lead to craniofacial malformations[50]. Overall, sequencing results showed that the *HOXD1* gene not only altered the extracellular matrix in neural crest cells, but also promoted bone differentiation. In summary, the CXC family may act as downstream regulators of the *HOXD1* gene, affecting cell migration by altering extracellular factors.

Conclusions

We successfully isolated NCCs from mouse embryos. Overexpression analysis revealed that the *HOXD1* gene could transform mouse neural crest primary cells into EMT transitional cells, impacting migrate ability without significantly affecting proliferation. Signaling pathway analysis suggested that *HOXD1* may inhibit NCC proliferation by modulating *Wnt* signaling rather than *TGF-β*. Transcriptome analysis indicated that the *HOXD1* gene influenced the extracellular matrix of CXC family regulatory cells and promoted neural crest cells differentiation. These findings provide a technology basis for molecular marker breeding of the sheep polycerate trait, and lay a theoretical foundation for further investigating growth regulation mechanism in multi-horned sheep. The results also provide experimental references for the study of *HOXD1* function in the embryonic growth and development of mammals.

Data availability

The raw reads of the NCCs transcriptome sequencing have been deposited into the GenBank database of the National Center for Biotechnology Information (PRJNA1216763).

Received: 17 January 2025; Accepted: 8 April 2025
Published online: 16 April 2025

References

1. Tiwari, M. et al. Deciphering genomic basis of unique adaptation of Ladakhi cattle to Trans-Himalayan high-altitude region of Leh-Ladakh in India. *Gene* **942**, 149251 (2025).
2. Ren, X. et al. A genome-wide association study identifies a genomic region for the polycerate phenotype in sheep (*Ovis aries*). *Sci. Rep.* **6**, 21111 (2016).
3. He, X. et al. Mapping the four-horned locus and testing the polled locus in three Chinese sheep breeds. *Anim. Genet.* **47**, 623–627 (2016).
4. Kijas, J. W., Hadfield, T., Naval Sanchez, M. & Cockett, N. Genome-wide association reveals the locus responsible for four-horned ruminant. *Anim. Genet.* **47**, 258–262 (2016).
5. Greyvenstein, O. F. C., Reich, C. M., Van Marle-Koster, E., Riley, D. G. & Hayes, B. J. Polyceraty (multi-horns) in Damara sheep maps to ovine chromosome 2. *Anim. Genet.* **47**, 263–266 (2016).
6. Zhang, H. et al. Novel heredity basis of the four-horn phenotype in sheep using genome-wide sequence data. *Animals* **13**, 3166 (2023).

7. Allais-Bonnet, A. et al. Analysis of polycerate mutants reveals the evolutionary co-option of *HOXD1* for Horn patterning in Bovidae. *Mol. Biol. Evol.* **38**, 2260–2272 (2021).
8. Paul, R., Peraldi, R. & Kmita, M. The pioneering function of the hox transcription factors. *Semin Cell. Dev. Biol.* **152–153**, 85–92 (2024).
9. Zákány, J., Fromental-Ramain, C., Warot, X. & Duboule, D. Regulation of number and size of digits by posterior hox genes: A dose-dependent mechanism with potential evolutionary implications. *Proc. Natl. Acad. Sci. U. S. A.* **94**, 13695–13700 (1997).
10. Wang, L. et al. Significance of HOXD transcription factors family in progression, migration and angiogenesis of cancer. *Crit. Rev. Oncol. Hematol.* **179**, 103809 (2022).
11. Cui, Y. et al. *HOXD1* functions as a novel tumor suppressor in kidney renal clear cell carcinoma. *Cell. Biol. Int.* **45**, 1246–1259 (2021).
12. Wen, X., Chen, Y. & Fang, X. Overexpression of *HOXD8* inhibits the proliferation, migration and invasion of breast cancer cells by downregulating ILP2 expression. *Exp. Ther. Med.* **22**, 1006 (2021).
13. Zhang, Y., Yu, Y., Su, X. & Lu, Y. HOXD8 inhibits the proliferation and migration of triple-negative breast cancer cells and induces apoptosis in them through regulation of AKT/mTOR pathway. *Reprod. Biol.* **21**, 100544 (2021).
14. Zhang, C. et al. The 4 bp deletion mutation in *HOXD1* gene determines the polycerate trait in Chinese Sishui fur sheep. *Anim. Genet.* **54**, 820–822 (2023).
15. Ba, H. et al. Single-cell transcriptome reveals core cell populations and androgen-RXFP2 axis involved in deer antler full regeneration. *Cell. Regen.* **11**, 43 (2022).
16. Capitan, A. et al. A newly described bovine type 2 scurs syndrome segregates with a frame-shift mutation in TWIST1. *PLoS One.* **6**, e22242 (2011).
17. Fan, X. et al. TWIST1 and chromatin regulatory proteins interact to guide neural crest cell differentiation. *ELife* **10**, e62873 (2021).
18. Yu, X. et al. Molecular mechanisms of TWIST1-regulated transcription in EMT and cancer metastasis. *EMBO Rep.* **24**, e56902 (2023).
19. Livak, K. J. & Schmittgen, T. D. Analysis of relative gene expression data using real-time quantitative PCR and the 2 (-Delta delta C(T)) method. *Methods* **25**, 402–408 (2001).
20. Kanehisa, M., Furumichi, M., Sato, Y., Kawashima, M. & Ishiguro-Watanabe, M. KEGG for taxonomy-based analysis of pathways and genomes. *Nucleic Acids Res.* **51**, D587–D592 (2023).
21. Kanehisa, M. Toward Understanding the origin and evolution of cellular organisms. *Protein Sci.* **28**, 1947–1951 (2019).
22. Kanehisa, M. & Goto, S. K. E. G. G. Kyoto encyclopedia of genes and genomes. *Nucleic Acids Res.* **28**, 27–30 (2000).
23. Zhang, M. et al. Investigate the odontogenic differentiation and dentin–pulp tissue regeneration potential of neural crest cells. *Front. Bioeng. Biotechnol.* **8**, 475 (2020).
24. Wang, Y. et al. Genetic basis of ruminant headgear and rapid antler regeneration. *Science* **364**, eaav6335 (2019).
25. Alkobtawi, M. et al. Characterization of pax3 and sox10 Transgenic xenopus laevis embryos as tools to study neural crest development. *Dev. Biol.* **444**, S202–S208 (2018).
26. Qin, T. et al. A population of stem cells with strong regenerative potential discovered in deer antlers. *Science* **379**, 840–847 (2023).
27. Li, C. & Suttie, J. M. Deer antlerogenic periosteum: A piece of postnatally retained embryonic tissue? *Anat. Embryol.* **204**, 375–388 (2001).
28. Wanninger, A. Hox, homology, and parsimony: an organismal perspective. *Semin. Cell. Dev. Biol.* **152–153**, 16–23 (2024).
29. Gaunt, S. J. *Hox* cluster genes and collinearities throughout the tree of animal life. *Int. J. Dev. Biol.* **62**, 673–683 (2018).
30. Gaunt, S. J. Seeking sense in the hox gene cluster. *J. Dev. Biol.* **10**(4). (2022).
31. Merabet, S. & Carnesecchi, J. *Hox* dosage and morphological diversification during development and evolution. *Semin. Cell. Dev. Biol.* **152–153**, 70–75 (2024).
32. Hoeven, F. V. D., Zákány, J. & Duboule, D. Gene transpositions in the *HoxD* complex reveal a hierarchy of regulatory controls. *Cell* **85**, 1025–1035 (1996).
33. Stern, D. L. A role of ultrabithorax in morphological differences between drosophila species. *Nature*. **396**, 463–466 (1998).
34. Refki, P. N. et al. Emergence of tissue sensitivity to *Hox* protein levels underlies the evolution of an adaptive morphological trait. *Dev. Biol.* **392** (2), 441–453 (2014).
35. Porcelli, D., Fischer, B., Russell, S. & White, R. Chromatin accessibility plays a key role in selective targeting of hox proteins. *Genome Biol.* **20**, 115 (2019).
36. Jung, H., Lacombe, J., Mazzoni, E. O., Liem, K. F. J. & Dasen, J. S. Global control of motor neuron topography mediated by the repressive actions of a single hox gene. *Neuron*. **67**, 781–796 (2010).
37. Zhao, R. & Trainor, P. A. Epithelial to mesenchymal transition during mammalian neural crest cell delamination. *Semin. Cell. Dev. Biol.* **138**, 54–67 (2023).
38. Gonzalez, V. D. et al. Commonly occurring cell subsets in high-grade serous ovarian tumors identified by single-cell mass cytometry. *Cell. Rep.* **22**, 1875–1888 (2018).
39. Karacosta, L. G. et al. Mapping lung cancer epithelial–mesenchymal transition States and trajectories with single-cell resolution. *Nat. Commun.* **10**, 5587 (2019).
40. Kumar, S. U., Kumar, D. T., Siva, R., Doss, C. G. P. & Zayed, H. Integrative bioinformatics approaches to map potential novel genes and pathways involved in ovarian cancer. *Front. Bioeng. Biotechnol.* **7**, 391 (2019).
41. Pastushenko, I. et al. Identification of the tumour transition States occurring during EMT. *Nature* **556**, 463–468 (2018).
42. Ramirez Moreno, M., Stempor, P. A. & Bulgakova, N. A. Interactions and feedbacks in e-cadherin transcriptional regulation. *Front. Cell. Dev. Biol.* **9**, 701175 (2021).
43. Bendall, L. Chemokines and their receptors in disease. *Histol. Histopathol.* **20**, 907–926 (2005).
44. Singh, S., Nannuru, K. C., Sadanandam, A., Varney, M. L. & Singh, R. K. CXCR1 and CXCR2 enhances human melanoma tumourigenesis, growth and invasion. *Brit J. Cancer*. **100**, 1638–1646 (2009).
45. Singh, S., Sadanandam, A., Varney, M. L., Nannuru, K. C. & Singh, R. K. Small interfering RNA-mediated CXCR1 or CXCR2 knock-down inhibits melanoma tumor growth and invasion. *Int. J. Cancer*. **126**, 328–336 (2010).
46. Zhou, C., Gao, Y., Ding, P., Wu, T. & Ji, G. The role of CXCL family members in different diseases. *Cell. Death Discov.* **9**, 212 (2023).
47. Wu, T., Yang, W., Sun, A., Wei, Z. & Lin, Q. The role of CXC chemokines in cancer progression. *Cancers* **15**, 167 (2022).
48. De Almeida, L. G. N. et al. Matrix metalloproteinases: from molecular mechanisms to physiology, pathophysiology, and pharmacology. *Pharmacol. Rev.* **74**, 714–770 (2022).
49. Chen, G. et al. BMP signaling in the development and regeneration of cranium bones and maintenance of calvarial stem cells. *Front. Cell. Dev. Biol.* **8**, 135 (2020).
50. Ueharu, H. & Mishina, Y. BMP signaling during craniofacial development: new insights into pathological mechanisms leading to craniofacial anomalies. *Front. Physiol.* **14**, 1170511 (2023).

Acknowledgements

We thank all the reviewers who participated in the review, as well as MJEditor (www.mjeditor.com) for providing English editing services during the preparation of this manuscript.

Author contributions

G.Y. and M.L. designed the research. C.Z., H.Z., T.D., L.T., M.C. and F.G. contributed to the experimental work. C.Z., S.Z., H.X. and G.W. performed the data analysis and wrote the manuscript. G.Y. and M.L. revised the manuscript. All authors reviewed and approved the manuscript.

Funding

This study was supported by the Research Program of Foundation and Advanced Technology of He'nan Science and Technology Committee of China (102300410143, 132300410398), the Key R&D and Promotion Program of He'nan Science and Technology Committee of China (252102110076), and the Foundation of He'nan Educational Committee of China (25A230006).

Declarations

Competing interests

The authors declare no competing interests.

Ethical approval

The animal care and use guidelines put forth by the Ministry of Science and Technology of China (Guidelines on Ethical Treatment of Experimental Animals (2006) No. 398) were followed for this study, with the Ethics Committee of Shangqiu Normal University having approved all experiments herein (Shang (2022) No. 24).

Additional information

Supplementary Information The online version contains supplementary material available at https://doi.org/10.1038/s41598-025-97865-9.

Correspondence and requests for materials should be addressed to M.L. or G.Y.